Original Research Article

Numerical Modelingof Tunnel Support System in Himalayan Rock Masses for Seismic Resilience

Abstract

This study uses numerical modeling in combination with rock mass classification approaches to develop tunnel support systems that are safe from earthquakes, ultimately contributing to the seismic resilience of the important infrastructure. A case study of tunnel in Himalayan region of Nepal has been considered for seismic assessment of tunnel supports in different geological conditions. For better quality rock masses (GSI>30), strain-softening model was used, and for weaker rock masses (GSI<30), elastic-perfectly-plastic model was used. To ensure safety in the case of extremely poor rock mass, shotcrete thickness had to be increased by 100 mm over that recommended by empirical methods. In both models, shotcrete in the sections with high overburden showed a significant decrease in FOS. Even though this type of unusual finding has also been reported in the Melamchi water supply tunnel after 2015 Gorkha Earthquake, no further studies to investigate the influencing factors have been done.While this condition occurred in the model used in this study because of the application of higher in-situ stress for sections with a larger depth of overburden, the actual reason for the occurrence of this situation as a result of an earthquake remains unexplained. Future research should take into account the effects of discontinuities,epicentral distance, aftershocks, and the incorporation of actual stress measurements from the field for numerical modeling.

Keywords: Seismic activity; tunnel support; earthquake resistance; geological settings; numerical modeling.

1 INTRODUCTION

Nepal has a long history of the occurrence of earthquakes of significant magnitude, as a result of which the construction sector has been putting extra efforts into building resilience in case of such disasters. Despite seismic challenges, Nepal's construction sector is expanding. The construction of tunnels in the hydropower industry is one of the sectors that is expanding despite these difficulties.According to information provided during the Nepal Tunneling Conference in 2019, 220 km of tunnel have been completed, while another 195 km are now being built as part of numerous active hydropower construction projects in Nepal[1].

Constructions underground have historically fared better than those on the surface[2]–[6]. This is because the soil and rock in the area impede the mobility of subsurface structures. The degree of redundancy of underground structures is greater than that of surface structures because underground structures are supported by the ground while surface structures are frequently unsupported above the ground[7]. Additionally, the increased modulus of elasticity with depth, the smaller excavation dimension relative to the much longer seismic wave length, and the reduction in ground motion amplitude with depth all contribute to the greater seismic resistance of underground structures[8].

Although tunnels are generally considered to be more resistant to seismic damage, many instances of such damage have been documented. Notable examples include the 1906 San

Francisco earthquake (Mw 7.9), the 1923 Great Kanto earthquake (Mw 7.9-8.2), and the 2008 Wenchuan earthquake (Mw 7.9), which all caused significant harm to mountain tunnels[9]–[13]. In the aftermath of the 2015 Gorkha earthquake (Mw 7.8) in Nepal, the Melamchi water supply project tunnel experienced cracks on its inside surface, wall, and crown[14], while Bhairabkunda Hydroelectric Project, Sindhupalchowk reported shotcrete cracking[15]. Such case histories demonstrate the crucial importance of incorporating seismic load considerations into the design of tunnel supports.

The main goal of this study is to assess the seismic performance of support elements and suggest support systems that are found to be seismic-resistant in terms of their factor of safety. Squeezing analysis has also been performed to predict time-dependent deformation.

2 METHODOLOGY

The goal of this research was to perform seismic assessment and suggest tunnel support systems that could withstand earthquakes in a variety of geological settings. This was accomplished through a series of consecutive tasks, including a review of the literature on earthquake damage and tunnel support design techniques. Data was collected for a case study from a variety of sources, including theses, data from project office, fieldwork, published articles, and lab work. After classifying the rock and soil, empirical techniques like Q and RMR were utilized to evaluate tunnel support. Following the calculation of the rock mass parameters, the tunnel's squeezing study was carried out. Tunnel support study was carried out utilizing Phase 2.0, a finite element modeling software. Finally, for every tunnel-related geological condition, an earthquake-resistant support was chosen. Figure 1 shows the flowchart of the methodology adopted for this study.

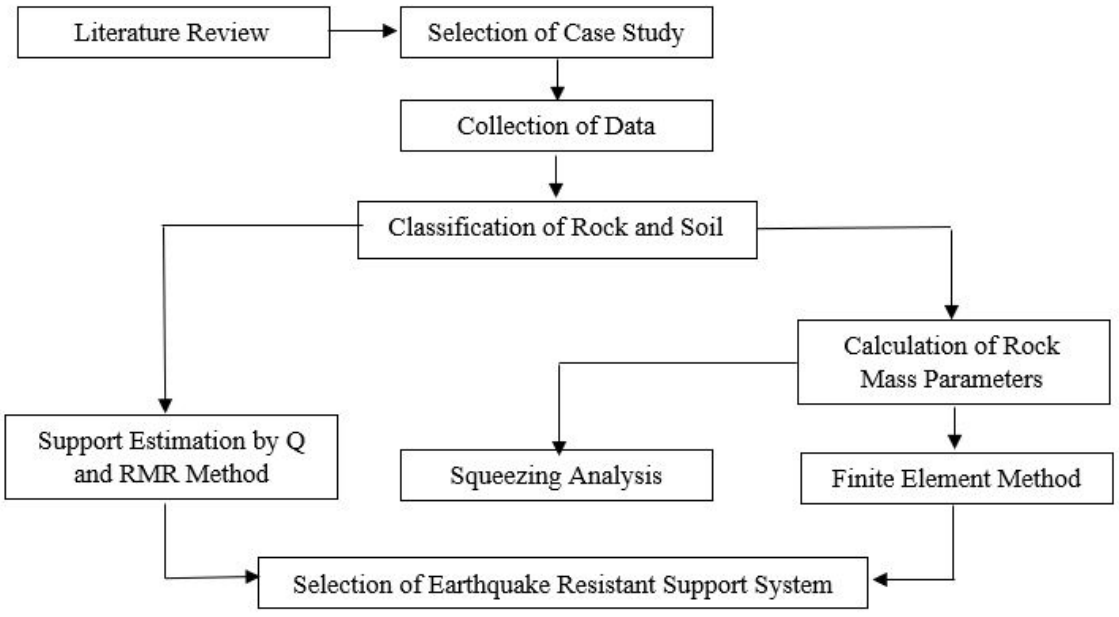

Figure 1: Methodology flowchart

3 PROJECT AREA

The Super Madi Hydro Electric Project (44 MW) is a run-of-river hydropower project located in the Madi Rural Municipality of Gandaki Province, Nepal. The headrace tunnel is an inverted D-shaped structure with an excavation size of 4.2 m× 4.2 m without pay line and functions as a low-pressure flow tunnel.

3.1 Geological Description

The Himalayan region is very favorable in terms of topography for hydropower construction. In most cases, headrace tunnels have been used for a safer and more economical structure for water conveyance. However, several challenges, such as poor rock mass quality, groundwater inflow, and squeezing conditions, interfere with the excavation process. The most commonly used construction techniques are the New Austrian Tunneling Method (NATM), the Norwegian Method of Tunneling (NMT), and excavation using Tunnel Boring Machines (TBM).

The headrace tunnel selected for our case study is located in Nepal's higher Himalayan region. The Main Central Thrust (MCT) is located at an aerial distance of about 2 km to the south of the powerhouse region [16]. The Higher Himalayan region consists of metamorphic rocks like precambrian gneiss, schist, and quarzite. Figure 2 shows the lithology of the tunnel's longitudinal section.

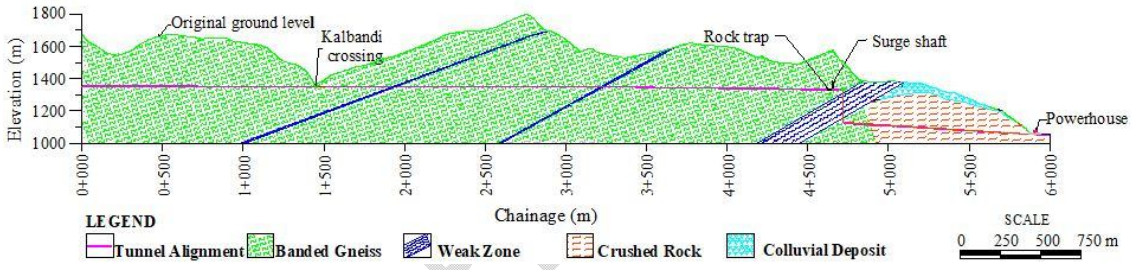

Figure 2: Longitudinal cross-section along the tunnel alignment

3.2 Study section 1

This section comprises chainages ranging from 1+000 m to 1+500 m and 3+600 m to 3+800 m. It consists of moderately weathered, fresh, medium-strong, foliated, gray-colored, medium-grained, banded gneiss. Quartz veins parallel to the foliation plane are present, while some are folded in sections 3+600 m to 3+800 m. Most of the rough, planar, freshly to moderately weathered joints have clay-filled apertures. The joints are closely to moderately spaced and have medium to high persistency with fair RQD. The rock's Q values range from 0.0038 for extremely poor rock to 1.25 for poor rock. The RMR values indicate the presence of fair rock (41–60) and poor rock (21–40).

3.3 Study section 2

The section between chainage 5+539 m and 5+547 m comprises heavily disintegrated gneiss, which is severely weathered and has transformed almost completely into residual soil. The soil's matrix is composed of a medium- to coarse-grained, silty clay, with a reddish-yellow to brownish color, and boulders are present on both faces and walls. The exceptionally poor rock mass present here has a Q value of 0.00416.Based on the laboratory tests on soil samples, the soil has been as clay with low plasticity (Figure 3).

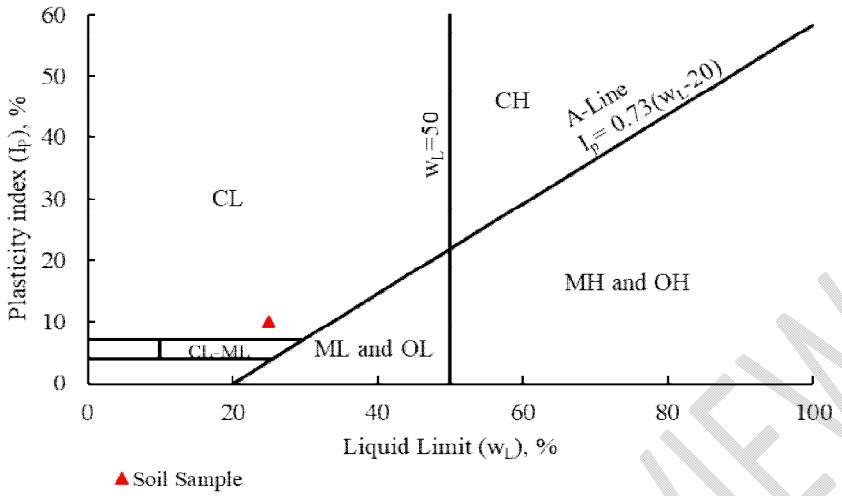

Figure 3: USCS classification of soil

4 ROCK MASS PARAMETERS

Vertical stresshas been calculated by the equation 1.

$$\sigma_v = \gamma z \quad (1)$$

Horizontal stress is given by equation 2[16].

$$\sigma_h = k \gamma z + \sigma_{tec} \quad (2)$$

The tectonic stress for the SMHEP is 6 MPa in the north-south direction, and the resolving components of tectonic stress along and perpendicular to the cavern alignment leading to the headrace tunnel are 1.29 MPa and 5.93 MPa, respectively[17].

The horizontal-to-vertical stress ratio is higher at a lesser depth due to the curvature of the earth, and the value is given by equation 3[18].

$$k = 0.25 + 7E\left(0.001 + \frac{1}{z}\right) \quad (3)$$

where E is the deformation modulus of earth crust in horizontal direction. According to Gautam[17], deformation modulus is taken as 3.97 GPa for banded gneiss. Values of k at different depths for banded gneiss are shown in Figure 4.

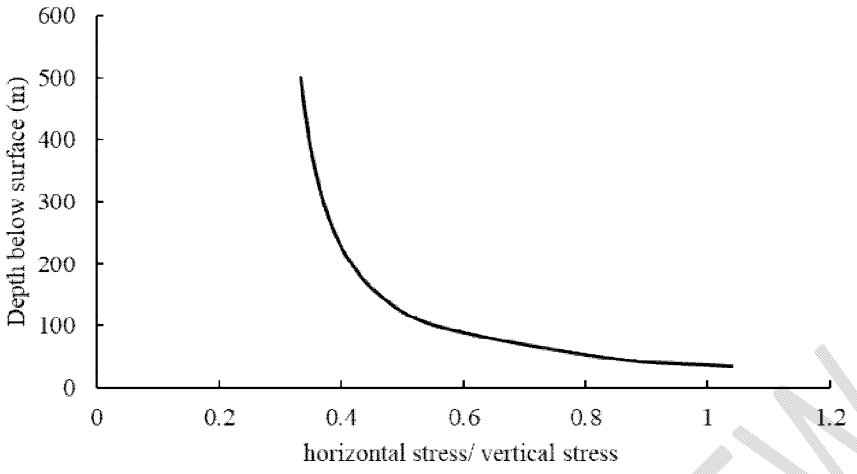

Figure 4: Variation of k with depth

The values of RMR, GSI, and E_{rm}were obtained from equations 4, 5, and 6, which were suggested by Barton[19], Hoek and Diederichs[20], and Hoek et al.[21], respectively. The intact strength of gneiss was taken as 130 MPa[17].

$$RMR = 15\log(Q) + 50 \quad (4)$$

$$GSI = RMR - 5 \quad (5)$$

$$E_{rm} = \left(1 - \frac{D}{2}\right) 10^{\frac{GSI-10}{40}} \quad (6)$$

The parameters of the rock mass on each of the study cross-sections have been provided in Table 1, while the parameters for numerical modeling are included in Table 2. For numerical modeling of rock, the disturbance factor is set to 0.8 to account for effects from the drill and blast method, while it is set to 0 for the section where soil predominates (Ch. 5+540 m).

Table 1: Rock mass parameters and rock mass classification for different chainages

Chainage (m)	Q	Q classification	RMR	RMR classification	GSI	E_{rm} (GPa)
1+000	0.344	Very poor rock	43	Fair rock	38	3.007
1+050	0.583	Very poor rock	46	Fair rock	41	3.574
1+100	0.229	Very poor rock	40	Poor rock	35	2.530
1+150	0.075	Extremely poor rock	33	Poor rock	28	1.691
1+200	0.038	Extremely poor rock	29	Poor rock	24	1.343
1+250	0.070	Extremely poor rock	33	Poor rock	28	1.691
1+300	1.250	Poor rock	51	Fair rock	46	4.766
1+350	1.083	Poor rock	51	Fair rock	46	4.766
1+400	0.271	Very poor rock	41	Fair rock	36	2.680
1+500	0.375	Very poor rock	44	Fair rock	39	3.185
3+600	0.500	Very poor rock	45	Fair rock	40	3.374
3+650	0.070	Extremely poor rock	33	Poor rock	28	1.691
3+700	0.038	Extremely poor rock	29	Poor rock	24	1.343

3+750	0.313	Very poor rock	42	Fair rock	37	2.839
3+800	0.344	Very poor rock	43	Fair rock	38	3.007
5+540	0.004	Exceptionally poor rock	14	Very poor rock	9	0.944

Table 2: Properties of rock and soil present in the study area

Banded Gneiss		Clayey Soil	
Poisson's Ratio	0.2	Poisson's Ratio	0.4
Unit Weight (KN/m^3)	27	Unit Weight (KN/m^3)	18.673
Disturbance Factor	0.8	Cohesive Strength (MPa)	0.096
Material Constant (m_i)	28	Friction Angle (Degree)	35
Failure Criteria	Generalized Hoek-Brown	Failure Criteria	Mohr-Coulomb

Figure 5 depicts the variation in overburden values (difference between the elevation of original ground level and elevation of top level of crown of tunnel) along the alignment. The overburden value is zero at the location of the Kalbandi river crossing, where water is conveyed from one side of the tunnel to the other with the help of a pipe of diameter 2.7 m.

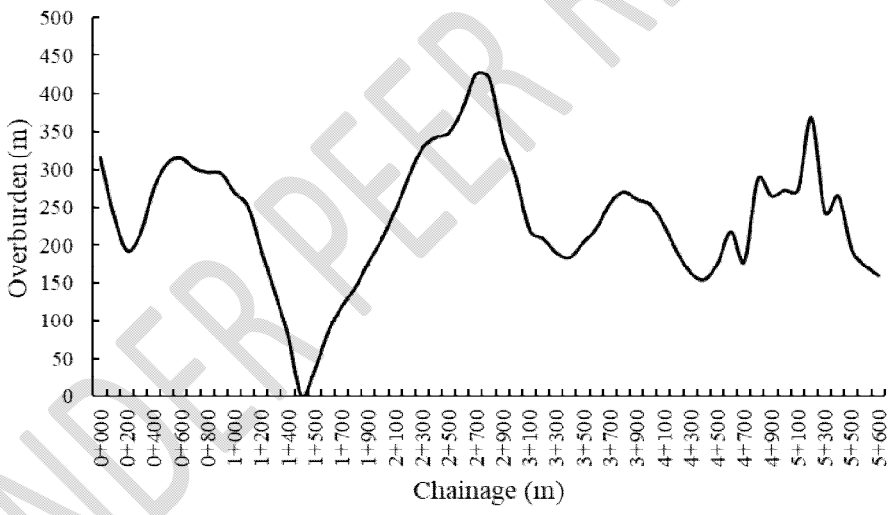

Figure 5: Overburden along the tunnel alignment

5 RESULT AND DISCUSSION

5.1 Squeezing Analysis

Squeezing ground condition is a time-dependent deformation that starts at excavation and can last for a period of time. This issue has been recorded in theChameliya Hydroelectric Project headrace tunnel[22], the Modi Khola pressure tunnel, and the Kaligandaki headrace tunnel[23]. Thus, for any tunnel constructed in Himalayan region, studying this phenomenon becomes crucial.

There are a number of empirical, semi-empirical, and semi-analytical methods to predict the possibility of squeezing. The Hoek and Marinos techniqueis a reliable method as it takes into account the effects of installation of tunnel support.

The findings of the squeezing analysis in study section 1 are presented in Figure 6. Since all the studied sections have a strain of less than one percent, it can be said that there is no possibility of squeezing. However, there are still chances of minor support problems.

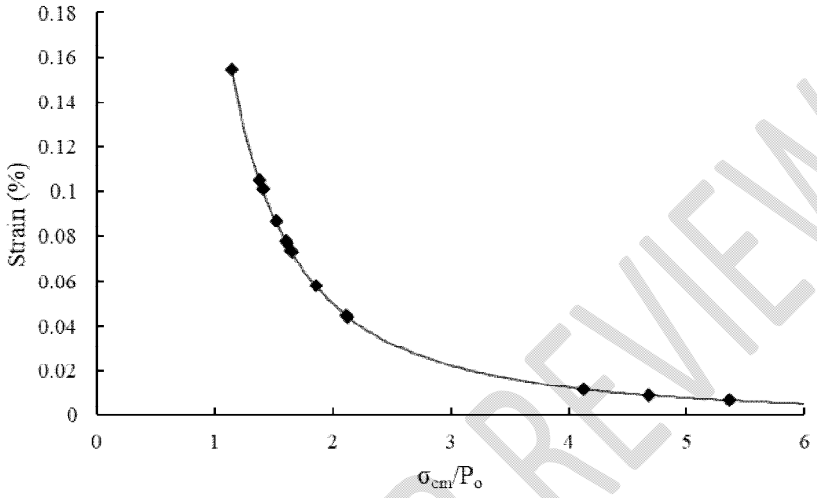

Figure 6: Tunnel strain vs σ_{cm}/P_0

5.2 Support estimation by empirical methods

Q and RMR methods were used to estimate the required tunnel supports. There is a recommended set of standard tunnel supports for specific values of RMR or Q. In the case of the Q method, supports have to be determined from the graph. The estimated supports for the studied sections from the Q and RMR methods are given in Tables 3 and 4, respectively.

Table 3: Tunnel supports calculated from Q method

Support Category	Description
4	Unreinforced shotcrete of thickness 40 to 100 mm and 2.4 m long bolts at 1.6 m spacing
5	Fiber reinforced shotcrete of thickness 50 to 90 mm and 2.4 m long bolt at 1.4 m spacing
7	Fiber reinforced shotcrete of thickness 120 to 150 mm and 2.6 m long bolt at 1.2 m spacing

The Q chart suggests three types of supports for the rock formations in study section 1. The stability of the sections with poor quality rock at Ch. 1+300 m and Ch. 1+350 m does not require any support. However, Ch. 1+050 m needs category 4 support, while chainages 1+000 m, 1+100 m, 1+400 m, 1+500 m, 3+600 m, 3+750 m and 3+800 m need category 5 support. Additionally, chainages ranging from 1+150 m to 1+250 m and 3+650 m to 3+700 m require support of category 7.

Table 4: Tunnel supports recommended by RMR method

RMR	Rock Type	Supports
41-60	Fair	50 to 100 mm thick shotcrete in crown, 30 mm thick shotcrete in sides, 4 m long bolts at 1.5 to 2m spacing, wire mesh in crown
21-40	Poor	100 to 150 mm thick shotcrete in crown, 100 mm thick shotcrete in sides, 4 to 5 m long bolts at 1 to 1.5 m spacing with wire mesh, light to medium steel ribs at 1.5 m spacing

5.3 Numerical Modeling

Numerical modelingwas done to evaluate the support needs for both static and seismic loading because the Q and RMR methods only estimate tunnel support requirements for static situations. Numerical modeling has been performed in Phase 2.0, a software for finite element analysis of excavations. The rock mass was modeled in two dimensions, considering that the tunnel is infinitely long. Chainages from study section 1 were modeledwith Hoek Brown failure criteria and those from study section 2 were modeled with Mohr-Coulomb failure criteria. The extent of external boundary was taken as four times of the tunnel diameter.Incorporating the same approach used by Abokhalil[24], boundary that restrains movement in both the X and Y directions was utilized to investigate the seismic response of the tunnel.Discretization was done with a six-noded triangle and the gradation factor was taken as 0.1. Figure 7 shows a representation of the 2D model.

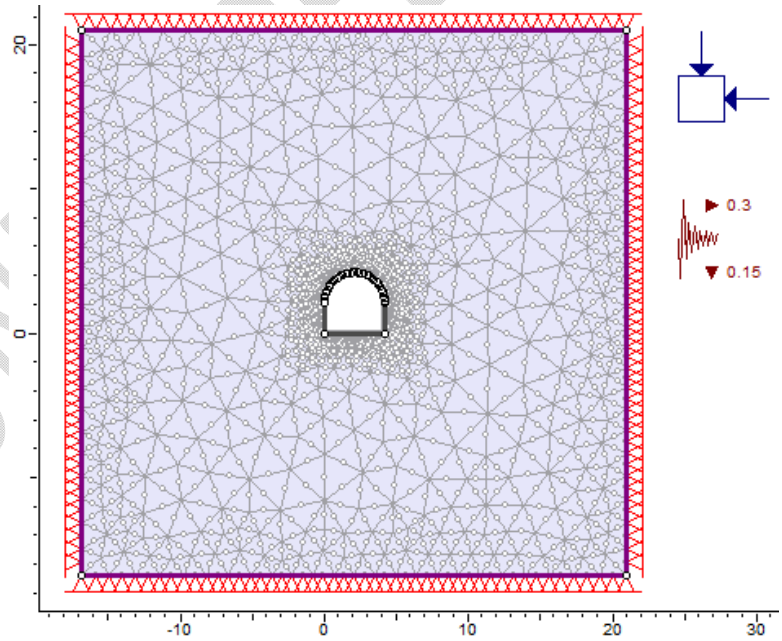

Figure 7: Finite element model showing mesh setup, static load and seismic load

As shown in Figure 8, internal pressure equal to in-situ stress was applied to the tunnel boundary and relaxed to zero in the tenth stage. The tunnel relaxation stage was then

determined usingVlachopoulos and Diederichs[25] method.That followed the support installation stage, and finally the seismic loading stage[26].

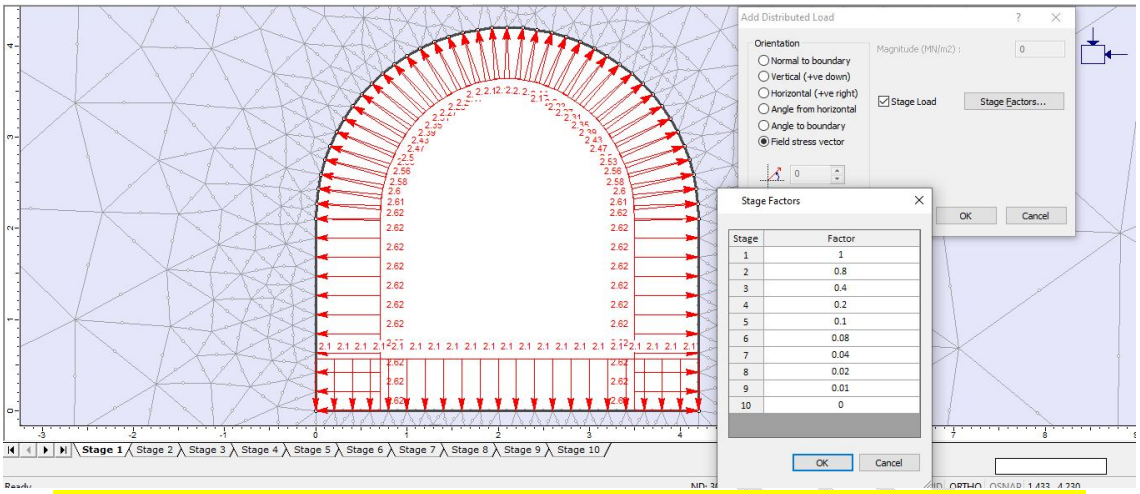

Figure 8: Application of uniformly distributed load showing stage factor in each stage

For the study ofthe effects of earthquakes on tunnels located in diverse geological conditions in the Himalayan region, a horizontal seismic coefficient of 0.3 and a vertical seismic coefficient of -0.15 are used[1] because maximum damage was observed in tunnels when peak horizontal acceleration was near 0.3g[27], [28], and maximum stresses were created on the tunnel perimeter when vertical seismic coefficient was acting downward[8]. For seismic analysis of tunnels, a vertical seismic coefficient equal to half of the horizontal seismic coefficient is used to partially account for the phaselag between the horizontal and vertical peak ground acceleration[29].

As the conclusion of a study conducted on six different hydropower tunnels in the Himalayan region, Khadka [30] stated that for better rock masses with GSI between 30 and 50, a strain-softening model with residual rock parameters set between 60 and 70% of peak values is suitable, and for rock masses with GSI lower than 30, an elastic-perfectly-plastic model is suitable. For this study, poor and very poor rock masses were modeled using a strain-softening model, whereas an elastic-perfectly-plastic model was used for extremely and exceptionally poor rock masses.

The supports, obtained from empirical methods, have been modified with the help of numerical model in such a way that the final support system is both optimal and lies within the factor of safety envelope for the given seismic load. The properties of shotcrete, rockbolt and steel rib used in the analysis are given in Table 5.Table 6 provides information about the set of supports satisfying the seismic resistance criteria for each rock mass class.

Table 5: Properties of liners used for numerical modeling

Shotcrete	
Compressive Strength	40 MPa
Beam Formulation	Timoshenko
Poisson's Ratio	0.15

Rockbolt	
Bolt Type	End Anchored
Diameter	20 mm
Bolt Modulus	200000 MPa
Tensile Capacity	0.1 MN
Steel Rib	
Grade	Fe 500

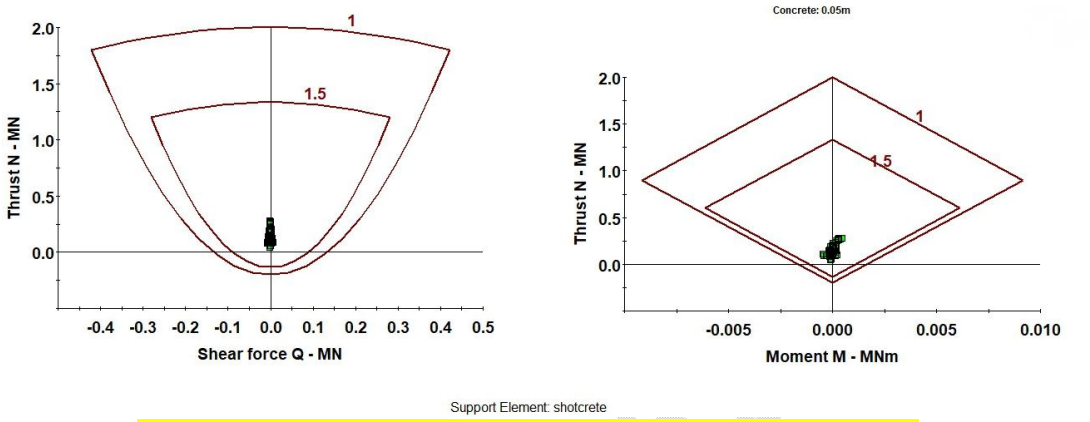

Figure 9: Support capacity plot of shotcrete at chainage 1+300 m

The poor rock at chainage 1+300 m was analyzed with a strain-softening model with residual parameters set to 68% of peak values. For easy installation, the bolt length has to be less than or equal to the span and height of the excavation[31]. Therefore, the bolt length for this rock class is fixed at 1.5 m, and 50 mm thick shotcrete is added.From Figure 9, no prominent difference is seen on the FOS of shotcrete between static and seismic conditions.

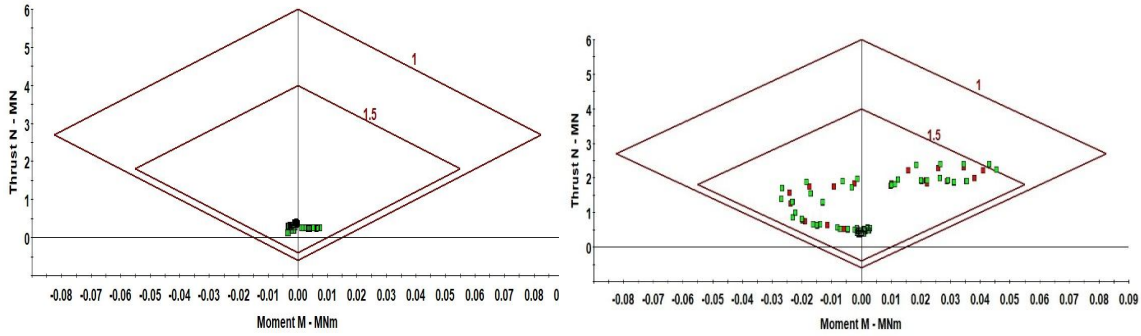

Figure 10: Support capacity plot of shotcrete at chainages 1+400 m (left) and 1+050 m (right) (red color representing liner elements in static condition and green color representing liner elements in seismic condition)

For very poor rock type at chainage 1+050 m, a strain-softening model was used with residual parameters set to 66% of the peak values. For chainage 1+400, which has overburden 184 m less than that of 1+050, residual parameters were set to 63% of the peak values.150 mm thick shotcrete and 1.5 m long bolts were used as supports for this rock type. As seen in Figure 10, the performance of 150 mm under seismic condition is better at section with lower overburden. At chainage 1+050 m, FOS of some shotcrete elements of the wall decreases

under seismic conditions and almost falls off the 1.5 FOS envelope. However, since theaddition of seismic did not cause any support element to yield, the selected support is considered to survive the simulated seismic activity.

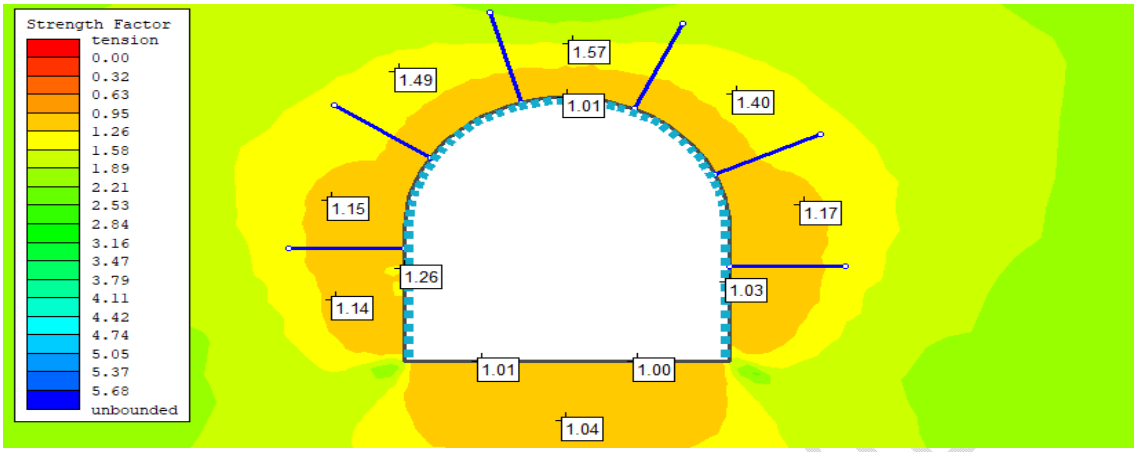

Figure 11: Strength factor around the tunnel at chainage 1+050 m

The strain-softening model for very poor rock showed that the FOS of shotcrete is lower on the walls at greater depth. This leads to the contradiction of existing literature, which reports lesser seismic damages to tunnels lying at greater depths. However, Shrestha et al. [14] observed the same case in their observation of damages to shotcrete in the Melamchi water supply tunnel after the 2015 Gorkha earthquake. They found a relatively larger number of damages to shotcrete in deeper sections. In the case of our study, the situation must have arisen due to the application of larger in-situ stresses at a higher depth (refer to equations 1 and 2).

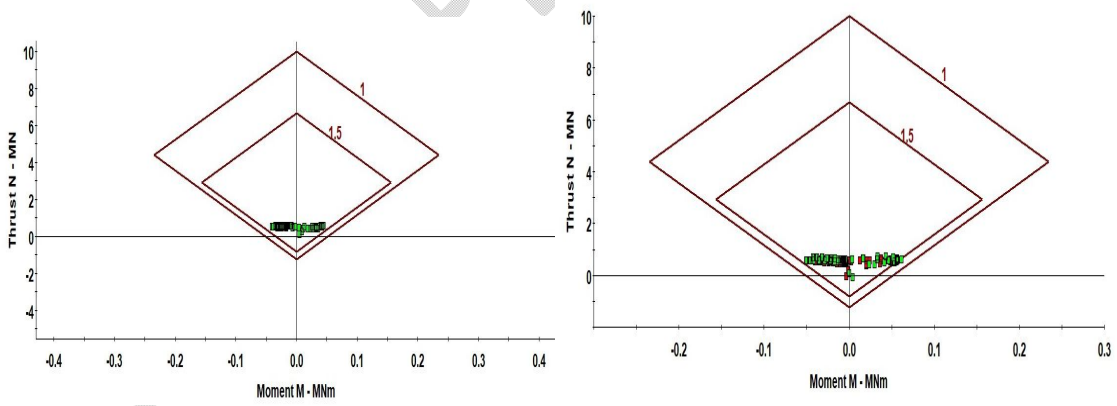

Figure 12: Support capacity plot of shotcrete at chainages 1+200 m (left) and 3+650 m (right) (red color representing liner elements in static condition and green color representing liner element in seismic condition

An elastic-perfectly-plastic model was used for modeling the extremely poor rock at chainages 1+200 m and 3+650 m. The span and height of the tunnel are only 4.2 m, so the use of 4 to 5 mlong bolts as suggested by the RMR approach is not feasible. Therefore, the length of the bolt in this rock type is limited to 2 m. This makes it necessary to use a shotcrete thickness of 250 mm in addition to the steel ribs at 1 m center-to-center spacing. This

thickness of shotcrete is 100 mm larger than recommended by empirical methods. Chainage 3+650 m has an overburden 47 m larger than that of chainage 1+200 m. As in the case of very poor rock, shotcrete in wall is found to have lower FOS in section with greater depth. However, in the absence of yielded support elements, the selected support system is considered safe for the simulated seismic activity.

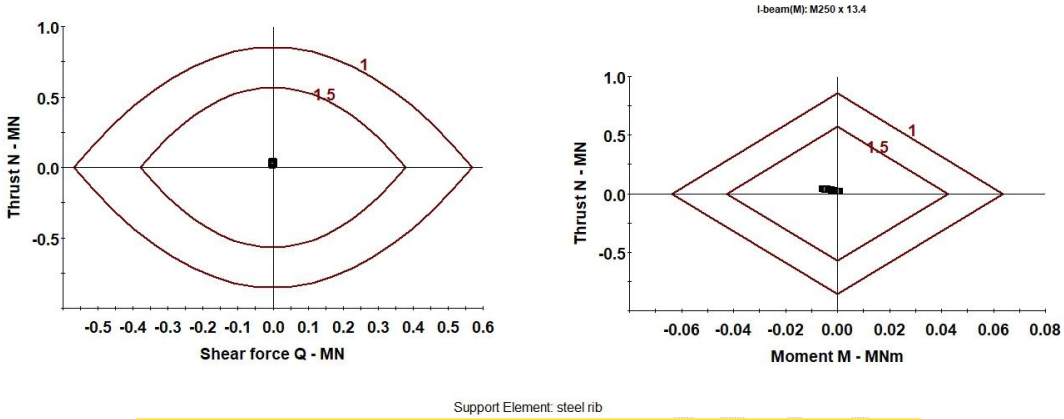

Figure 13: Support capacity plot of steel rib at chainage 5+540 m

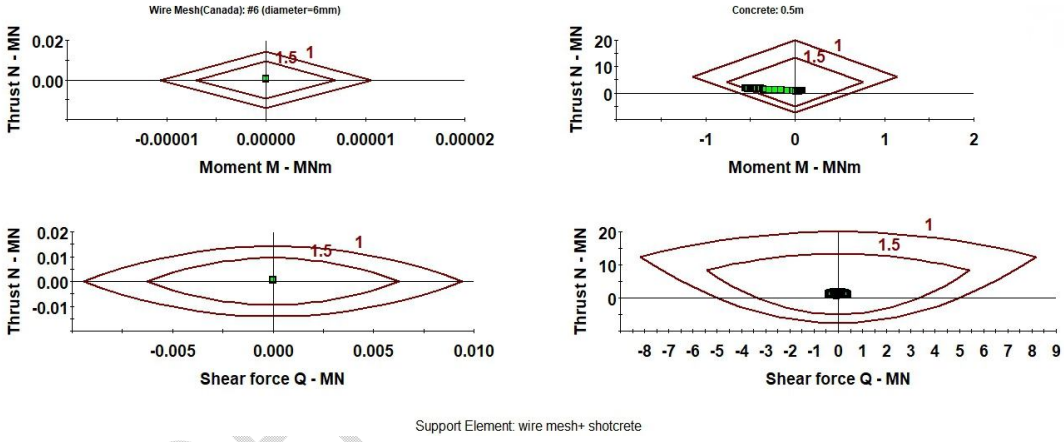

Figure 14: Support capacity plot of wire mesh and shotcrete at chainage 5+540 m

An elastic-perfectly-plastic model was used to analyze the seismic performance of supports in the case of exceptionally poor rock mass at chainage 5+540 m. Since the section is dominated by the presence of clayey soil, use of supports recommended by Q and RMR methos were not applied. Rock bolt was not found to be efficient in this type of rock mass. So, wire mesh filled with 500 mm thick shotcrete was used. On addition of M250×13.4 steel ribs at 0.5 center-to-center spacing, the section was found safe in the absence of yielding of liner elements. Tectonic stress was not taken into account for this rock mass. From the model, it was found that the FOS of shotcrete was lower on the crown than in the walls.

Table 6: Final earthquake resistant supports for different geological conditions

Rock Type	Q value	Supports
Poor	1-4	Fiber reinforced shotcrete of 50 mm thickness, 1.5 m long rockbolt at 1.5×1.5 m spacing
Very Poor	0.1-1	Fiber reinforced shotcrete of 150 mm thickness, 1.5 m long rockbolt at 1.5×1.5 m spacing
Extremely Poor	0.01-0.1	Fiber reinforced shotcrete of 250 mm thickness, 2 m long rockbolt at 1.5×1.5 m spacing, M100×6.1 steel rib at 1m spacing
Exceptionally poor rock with the predominance of soft soil	-	6 mm diameter wire mesh with 200 mm spacing filled with 500 mm thick fiber reinforced shotcrete, M250×13.4 steel rib at 0.5m spacing

6 CONCLUSION

This study focused on the seismic analysis and optimization of tunnel support systems for varied geological settings in the Himalayan region using numerical modeling. The preliminary estimation of supports was done with the help of rock mass classification methods like Q and RMR. Then, better rock masses (GSI>30) were modeled with a strain-softening model, while poorer rock masses (GSI<30) were modeled with an elastic-perfectly-plastic model. It was found that the empirical methods frequently underestimated or overestimated the tunnel support elements, with the suggested length of rock bolts being larger than the span and height of the tunnel in some cases. In case of extremely poor rock mass, an increment of shotcrete up to 100 mm was required to ensure safety.

From both the material models, it was observed that shotcrete at sections with higher overburden experienced higher seismic impacts. In sections at deeper locations, the FOS of the shotcrete liner at the wall region was found to be lower under seismic loading in very poor and extremely poor rock mass. However, this study could only assume higher in-situ stress at deeper locations as the reason for this. Since this study is limited due to the reliance on tectonic stress values from previous literature, the exclusion of rock discontinuities, and the effects of aftershocks and nearer epicenters, the findings cannot totally explain this phenomenon. Therefore, further research utilizing advanced programs and simulations is necessary to accurately determine the reason for the occurrence of this phenomenon, considering the combined effects of multiple factors, which have been presented as the shortcomings of this study.

REFERENCES

[1] S. Sapkota and G. B. Motra, "Seismic Impacts on Tunnels in Different Rock Mass," in *Proceedings of 10th IOE Graduate Conference*, Oct. 2021, pp. 61–67.

[2] Y. M. A. Hashash, J. J. Hook, B. Schmidt, and J. I-Chiang Yao, "Seismic design and analysis of underground structures," *Tunnelling and Underground Space Technology*, vol. 16, no. 4, pp. 247–293, Oct. 2001, doi: 10.1016/S0886-7798(01)00051-7.

[3] L. Li, L. Xian, C. Yao, D. Guo, and C. Liu, "Numerical Modeling of Seismic Responses and Seismic Measures of Tunnel Crossing a Fault Zone: A Case Study," *Advances in Materials Science and Engineering*, vol. 2020, pp. 1–12, Apr. 2020, doi: 10.1155/2020/5640561.

[4] J. Takemura, C. Yao, and O. Kusakabe, "Development of a fault simulator for soils under large vertical stress in a centrifuge," *International Journal of Physical Modelling in Geotechnics*, vol. 20, no. 3, pp. 118–131, May 2020, doi: 10.1680/jphmg.18.00010.

[5] C. Yao and J. Takemura, "Using laser displacement transducer scanning technique in centrifuge modeling of reverse fault–foundation interaction," *Soil Dynamics and Earthquake Engineering*, vol. 121, pp. 219–232, Jun. 2019, doi: 10.1016/j.soildyn.2019.03.018.

[6] C. Yao and J. Takemura, "Centrifuge Modeling of Single Piles in Sand Subjected to Dip-Slip Faulting," *Journal of Geotechnical and Geoenvironmental Engineering*, vol. 146, no. 3, Mar. 2020, doi: 10.1061/(ASCE)GT.1943-5606.0002202.

[7] J.-N. Wang and G. A. Munfakh, "Seismic Design Of Tunnels," *WIT Transactions on the Built Environment*, vol. 57, 2001.

[8] T. K. Sivarajan, "Seismic load considerations in the design of underground structures for hydropower projects in the Himalayan region," in *Proceedings of the conference on Recent Advances in Rock Engineering (RARE 2016)*, Paris, France: Atlantis Press, 2016. doi: 10.2991/rare-16.2016.54.

[9] X. Zhang, Y. Jiang, and K. Maegawa, "Mountain tunnel under earthquake force: A review of possible causes of damages and restoration methods," *Journal of Rock Mechanics and Geotechnical Engineering*, vol. 12, no. 2, pp. 414–426, Apr. 2020, doi: 10.1016/j.jrmge.2019.11.002.

[10] H. Yu, Y. Yuan, and A. Bobet, "Seismic analysis of long tunnels: A review of simplified and unified methods," *Underground Space*, vol. 2, no. 2, pp. 73–87, Jun. 2017, doi: 10.1016/j.undsp.2017.05.003.

[11] G. Tsinidis*et al.*, "Seismic behaviour of tunnels: From experiments to analysis," *Tunnelling and Underground Space Technology*, vol. 99, p. 103334, May 2020, doi: 10.1016/j.tust.2020.103334.

[12] K. Dehghanian, "Analytical Method for Preliminary Seismic Design of Tunnels," in *Theory and Practice of Tunnel Engineering*, IntechOpen, 2022. doi: 10.5772/intechopen.97634.

[13] Y. Shen, B. Gao, X. Yang, and S. Tao, "Seismic damage mechanism and dynamic deformation characteristic analysis of mountain tunnel after Wenchuan earthquake," *Eng Geol*, vol. 180, pp. 85–98, Oct. 2014, doi: 10.1016/j.enggeo.2014.07.017.

[14] R. Shrestha, X. Li, L. Yi, and A. K. Mandal, "Seismic Damage and Possible Influencing Factors of the Damages in the Melamchi Tunnel in Nepal Due to Gorkha Earthquake 2015," *Geotechnical and Geological Engineering*, vol. 38, no. 5, pp. 5295–5308, Oct. 2020, doi: 10.1007/s10706-020-01364-9.

[15] S. C. Sunuwar, "Nepal Earthquake 25 April 2015: Hydro projects damaged, risks and lessons learned for design considerations," *Journal of Nepal Geological Society*, vol. 55, no. 1, pp. 141–149, Jun. 2018, doi: 10.3126/jngs.v55i1.22804.

[16] C. B. Basnet and K. K. Panthi, "Evaluation on the Minimum Principal Stress State and Potential Hydraulic Jacking from the Shotcrete-Lined Pressure Tunnel: A Case from Nepal," *Rock Mech Rock Eng*, vol. 52, no. 7, pp. 2377–2399, Jul. 2019, doi: 10.1007/s00603-019-1734-z.

[17] U. Gautam, "Stability Assessment of the Underground Settling Basin Cavern of Super Madi Hydroelectric Project, Nepal," Master Thesis, Norwegian University of Science and Technology, Trondheim, 2012.

[18] P. R. Sheorey, "A theory for In Situ stresses in isotropic and transverseley isotropic rock," *International Journal of Rock Mechanics and Mining Sciences & Geomechanics Abstracts*, vol. 31, no. 1, pp. 23–34, Feb. 1994, doi: 10.1016/0148-9062(94)92312-4.

[19] N. Barton, "The influence of joint properties in modelling jointed rock masses.," in *8th ISRM Congress*, Apr. 1995, pp. 1023–1032.

[20] E. Hoek and M. S. Diederichs, "Empirical estimation of rock mass modulus," *International Journal of Rock Mechanics and Mining Sciences*, vol. 43, no. 2, pp. 203–215, Feb. 2006, doi: 10.1016/j.ijrmms.2005.06.005.

[21] E. Hoek, C. Carranza-Torres, and B. Corkum, "Hoek-Brown failure criterion-2002 Edition," in *Proceedings of North American Rock Mechanics Society Meeting*, Toronto, 2002, pp. 267–273.

[22] P. K. Shrestha, K. K. Panthi, and C. B. Basnet, "Analysis of Squeezing Phenomenon in the Headrace Tunnel of Chameliya Project, Nepal," *Hydro Nepal: Journal of Water, Energy and Environment*, vol. 13, pp. 44–51, Mar. 2014, doi: 10.3126/hn.v13i0.10039.

[23] K. K. Panthi, "Analysis of Engineering Geological Uncertainties Related to Tunnelling in Himalayan Rock Mass Conditions," PhD Thesis, Norwegian University of Science and Technology, Trondheim, 2006.

[24] M. Abokhalil, "Insights into the Response of Rock Tunnels to Seismicity," Master Thesis, University of Oslo, Oslo, 2007.

[25] N. Vlachopoulos and M. S. Diederichs, "Improved Longitudinal Displacement Profiles for Convergence Confinement Analysis of Deep Tunnels," *Rock Mech Rock Eng*, vol. 42, no. 2, pp. 131–146, Apr. 2009, doi: 10.1007/s00603-009-0176-4.

[26] A. Srivastav, “Seismic Response of Rock Tunnels in Mixed Himalayan Geology,” PhD Thesis, International Institute of Information Technology, Hyderabad, 2022.

[27] S. Sharma and W. R. Judd, “Underground opening damage from earthquakes,” *Eng Geol*, vol. 30, no. 3–4, pp. 263–276, Jun. 1991, doi: 10.1016/0013-7952(91)90063-Q.

[28] N. Roy and R. Sarkar, “A Review of Seismic Damage of Mountain Tunnels and Probable Failure Mechanisms,” *Geotechnical and Geological Engineering*, vol. 35, no. 1, pp. 1–28, Feb. 2017, doi: 10.1007/s10706-016-0091-x.

[29] T. Tshering, “The Impact of Earthquakes on Tunnels in different Rock Mass Quality Q: A numerical analysis,” Master Thesis, University of Oslo, Oslo, 2011.

[30] S. S. Khadka, “Tunnel Closure Analysis of Hydropower Tunnels in the Lesser Himalayan Region of Nepal through Case Studies,” PhD Thesis, Kathmandu University, 2019. doi: 10.13140/RG.2.2.35884.41607.

[31] C. C. Li, “Principles of rockbolting design,” *Journal of Rock Mechanics and Geotechnical Engineering*, vol. 9, no. 3, pp. 396–414, Jun. 2017, doi: 10.1016/j.jrmge.2017.04.002.

Symbols and Abbreviations

Mw	Moment Magnitude	P_0	In situ Stress
MW	Mega Watt	E_{rm}	Rock Mass Elastic Modulus
FOS	Factor of Safety	D	Disturbance Factor
Q	Rock Mass Quality	Z	Overburden
RMR	Rock Mass Rating	K	Stress Ratio
RQD	Rock Quality Designation	σ_v	Vertical Pressure
GSI	Geological Strength Index	σ_h	Horizontal Pressure
USCS	Unified Soil Classification System	σ_{tec}	Tectonic Stress
σ_{cm}	Strength of Rock Mass	γ	Unit Weight